Autonomous Rover Enables Radar Profiling of Ice-Fabric Properties in Antarctica

M. Reza Ershadi, Reinhard Drews, Jonathan Hawkins, Joshua Elliott, Austin P. Lines, Inka Koch, and Olaf Eisen

***Abstract*—Ground-penetrating radar is an extensively used geophysical tool in cryosphere sciences (ice sheets and glaciers) with sounding depths of several kilometers due to the small radio-wave attenuation in ice sheets. Detection of the ice thickness and internal ice stratigraphy with commercial radars has become standard. However, there is still an observational gap in determining dielectric and mechanical ice-fabric anisotropy and basal properties using these systems. Recently, ground-based phase coherent radar has been showed its potential to fill this gap. However, this requires that the corresponding ground-based radars cover profiles several tens of kilometers in length. We address this challenge by modifying an autonomous rover to collect phase-coherent, quad-polarimetric radar data geolocated with real-time kinematic positioning. In a proof-of-concept study in Antarctica, we demonstrate that this allows the collection of quad-polarimetric data along a 23 km profile, mapping anisotropic ice-fabric properties at <100 m intervals across the transition of grounded to floating ice. This study shows the possibility of collecting data that will refine ice-flow models by providing missing rheological parameters. This work also demonstrates the versatility of the autonomous ground vehicle with its ability to tow more than 200 kg payload, with a battery run time of over six hours, and with a modular design that enables future integration of different radars or other geophysical sensors.**

***Index Terms*—Rover, Anisotropy, Radar, pRES, Antarctica.**

I. Introduction

Ice flow models predicting Antarctica's contribution to future sea level rise typically apply an isotropic rheology [1], although it is known that ice is mechanically anisotropic [2]. One reason why anisotropic rheology is not yet operationally implemented lies in insufficient observations which could spatially constrain anisotropic ice properties. The best observations are currently restricted to point information from ice cores taken predominantly from Antarctica's interior [2], [3]. Radar and seismic surveys have been developed as an additional tool to estimate lower resolution ice-fabric anisotropy away from ice cores [4]–[13], however, so far those approaches are also limited to point measurements.

A promising instrument to constrain anisotropic ice properties is the Autonomous phase-sensitive Radio Echo Sounder (ApRES) [14], [15]. Here, this is referred to as pRES since the autonomous mode is not used. pRES has had success in various other applications including determination of basal melt rates [16], firn compaction rates [17], vertical strain rates [18], and the Glen flow index [19], and can also be used to infer horizontal ice-fabric anisotropy from quad-polarimetric data [9]–[12], [20]. However, the pRES was originally designed exclusively for stationary operations, limiting its versatility in obtaining spatially distributed data. In previous studies [10]–[12], the spatial coverage was limited to selected profiles with < 10 km in length and with a sampling interval typically >500 m. This often makes it difficult to trace polarimetric (and hence ice-fabric) signatures spatially across different flow regimes. Here we combine the pRES with an autonomous rover so that ice-fabric properties can be infered along longer and more densely spaced profiles from quad-polarimetric radar data.

Radar data has been collected by autonomous rovers both in the Arctic [21]–[23] and the Antarctic [24]. While there are examples of coherent radars being deployed in this way [25], [26], many of these efforts rely on commercial, incoherent radars. These are excellent tools, e.g., for tracing internal layers [27] and/or crevasse detection, but they have limitations in resolving properties such as ice-fabric anisotropy because the received signal phase is not recorded. This limits the applicability of polarimetric surveys as done here, but also of other applications such as synthetic aperture radar processing relevant for smaller-scale processes such as basal terracing [28] or subglacial conduit formation [29], [30].

To address these limitations, we introduce SLEDGE, a **S**elf-guided four-whee**L**ed rov**E**r for ra**D**ar profilin**G** on ic**E**, designed to (1) collect quad-polarimetric radar data with pRES radar along pre-defined tracks several tens of kilometers in length, (2) collect radar data with other phase-coherent radars suitable for SAR processing (not shown here) requiring a sub-dm positioning along profiles more than several hundreds of meters in length, and (3) enable different measuring modes during profiling through integration of the rover and radar. Here, we use a multiple-input multiple-output (MIMO) pRES and integrate it into SLEDGE to autonomously map the ice base, detect internal layers, and, most significantly, acquire polarimetric data for inferring ice fabric properties (section II). We then present the results of a first deployment on the Ekström ice shelf in East Antarctica (section III) and report our test and field observations of SLEDGE for future development (section III-D).

M. Reza Ershadi, Reinhard Drews and Inka Koch are with the Department of Geosciences, University of Tübingen, DE (email:mohammadreza.ershadi@uni-tuebingen.de).

Jonathan Hawkins is with the School of Earth and Environmental Sciences, Cardiff University, Cardiff, UK.

Joshua Elliott and Austin P. Lines are with Polar Research Equipment, Etna, NH, US.

Olaf Eisen is with Alfred Wegener Institute, Helmholtz Centre for Polar and Marine Research, Bremerhaven, DE and Department of Geosciences, University of Bremen, Bremen, DE.

II. SLEDGE

A. Overview

The key components of SLEDGE (Fig. 1) include a four-wheeled rover equipped with a mini-industrial computer, two Cross Fox Sleds made of ultra-high-molecular-weight polyethylene holding a pRES radar and four antennas, two GNSS navigation systems mounted on the rover, and a control station. The rover can drive, self-guided, to predefined locations and then trigger radar data acquisition. The design of SLEDEGE is modular, having sufficient space, ports, power and weight capacity for additional sensors such as camera, a laser scanner, or other geophysical sensors. Here, only a pRES radar with a quad-polarimetric antenna setup will be shown. In terms of the driving mechanics, we rely on a commercially available rover, FrostyBoy (section II-B). We modified some hardware and the entire software to facilitate radar and GNSS sensor integration (section II-B). The commercial names, models, and information of the main components of SLEDGE are presented in the Supporting Information Sec. 5.

B. Rover

The FrostyBoy rover, which SLEDGE is built on, is manufactured by Polar Research Equipment and its hardware is described in [23], [31]. This four-wheeled rover features four individual brushless DC electric motors, each with a 40:1 planetary gearbox, allowing for independent propulsion. Two motor controllers are used to manage the front and rear motors, which, according to our test, allow the rover to tow more than 200 kg on ice. The payload in our case was roughly 100 kg (incl. two sledges (2x30 kg) and the radar system (40 kg)). FrostyBoy is equipped with a radio transceiver and antenna for receiving commands and transmitting telemetry, along with a GNSS system for coarse navigation with a horizontal accuracy of approximately 3 m. At the core of the rover's electronic system is an Arduino microcontroller development board. The power supply is facilitated by seven lithium-ion (Li-ion) battery modules, collectively providing an approximate total voltage of 56 V and providing battery run time of over six hours. Within a waterproof and insulated enclosure are the rover's electronics, motor controllers, and batteries, while the radio and GNSS antennas are externally mounted (Fig. 1).

The control station associated with FrostyBoy is a Windows computer equipped with essential peripherals, radio transceiver, and antenna. It operates on a power supply provided by two Li-ion batteries, offering a $\sim$16 V voltage output that can be replenished through solar charging. The entire control station setup is enclosed within a waterproof case to ensure protection. Effective communication (up to 7 km line of sight) between the control station and the rover is facilitated by a 900 MHz radio modem, enabling the transmission of commands from the operator to the rover and real-time telemetry data at the control station. The real-time GPS described in section II-C uses its own communication link.

For SLEDGE, we implemented some hardware and complete software changes to FrostyBoy. We added an industrial-grade mini-computer that integrates the required I/O ports for the other system components. This reduces the necessity for additional electronic components with the cost of some rewiring. We kept the Arduino board due to its flexibility for communication with the motor controllers. Although adding an industrial-grade mini-computer increases power consumption, it enables the use of Robotic Operating System version 2 (ROS2) - Foxy [32] as a standardized option for hardware communications providing an interface to a suite of external sensors (Supporting Information Sec. 1). To facilitate external access to all the available ports without compromising the rover's internal electronics,

we installed a dedicated interface panel on the left side of the rover which exposes internal I/O ports. This panel enables direct connection of external devices, such as radar systems, a secondary GNSS system, cameras, lights, and display, to the main computer. While the hardware of the control station remains unchanged, we have developed a new MATLAB® Graphical User Interface (GUI) (Supporting Information Sec. 2). Through the new GUI, the operator can communicate with the rover, switch between navigation systems, manually control the radar, and design different types of radar surveys.

C. GNSS-based Navigation

SLEDGE connects to two GNSS systems simultaneously and chooses between them from the control station based on the type of survey. FrostyBoy came with a standard 19x HVS Garmin® GNSS unit mounted on top of the rover suitable for a survey where a sensor-limited positional accuracy of 3 m can be tolerated. However, to achieve the sub-dm positioning envisaged for future SAR surveys we used a Real-Time Kinematic (RTK) GNSS unit including two antennas and receivers (base and rover). Having a receiver connected to each GNSS antenna is necessary since the accurate positions are calculated relative to a coarsely determined base station location and transmitted to the rover receiver for corrections via radio connection (403-473 MHz) resulting in improved positioning accuracy (8 mm horizontal, 15 mm vertical). The base antenna and its receiver are positioned on a tripod (fixed position) while the rover antenna and its receiver are mounted on the top and right side of the rover, respectively. A range of 1 km line of sight is required in order to maintain the radio connection between the base and the rover. An RTK signal booster (repeater) between the base and rover can be used if longer distances are necessary.

D. Polarimetric pRES Measurements

In the SLEDGE setup, we integrated a polarimetric version of pRES radar [14], [15] developed by the British Antarctic Survey (BAS) and University College London (UCL). The pRES transmits a linear, frequency-modulated continuous wave (FMCW) chirp with a frequency bandwidth of 200 MHz, centered at 300 MHz. It employs linearly polarized skeleton slot antennas, which exhibit peak directivity in the nadir (ice-facing) direction. To enable polarimetric measurements and avoid the need for mechanical rotation of the antennas, multiplexers were installed at the transmitter output and receiver input to select pairs of antennas with desired polarization

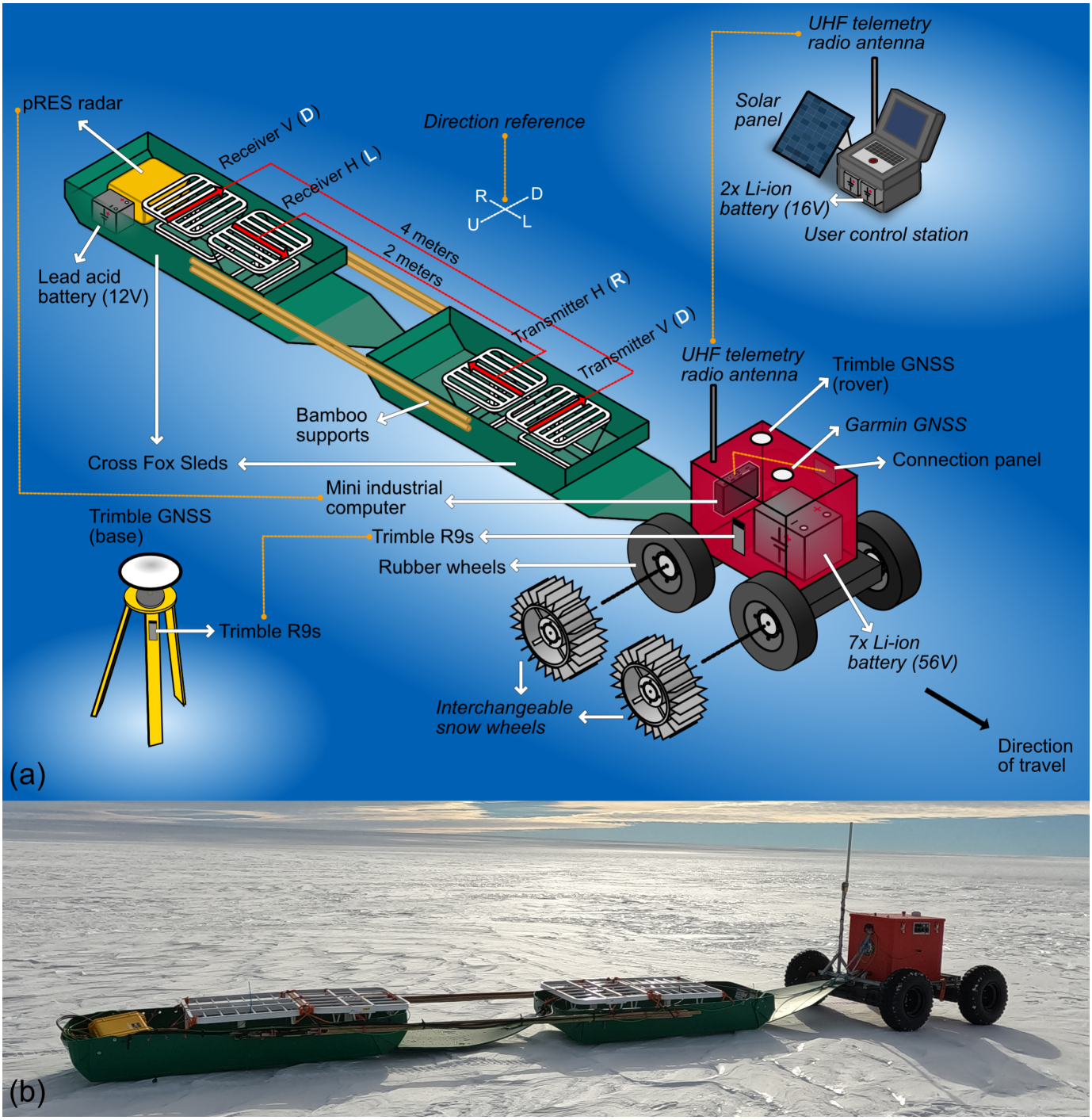

Fig. 1. (a) Schematic of SLEDGE. The red arrows on the radar antennas show the direction of the electrical field. The dashed yellow lines represent the communication between the two devices. Note that the figure is not to scale. The UHF telemetry and the rover (incl. wheels, power supply and driving system) are provided by Polar Research Equipment. (b) Photograph from DATE of the implementation as used on Ekströmisen, Antarctica.

characteristics. Because the antennas are multiplexed, rather than unique channels, measurements from each transmit-receive pair are recorded sequentially which results in an increased observation time of several seconds proportional to the number of antenna combinations at each site. While a total of four antennas (2 Tx, 2 Rx) are used in experiments described here, this is extendable to a total of 8 transmit and 8 receive antennas. To facilitate pRES measurments at pre-defined locations, we integrated the pRES into the SLEDGE setup by mounting it, along with its antennas, inside two plastic sleds located at the rear of the rover (Fig. 1). The pRES box and antennas were fixed securely within the sleds using a rope and connected to the back of the rover for ease of towing. Communication between the pRES and the rover's computer is facilitated by a wired Ethernet link and HTTP REST API, which allows for the radar to be triggered at pre-

defined waypoints, real-time configuration of the radar receiver settings, and backup of recorded measurements to the rover's computer.

The orientation of the pRES antennas is important because the propagation velocity of the electromagnetic wave in ice is orientation-dependent [4], [5], [33]. This information is used for polarimetric data processing and ice-fabric analysis. Following notation used in satellite remote sensing literature, we refer to the two orthogonal polarizations as horizontal (H) and vertical (V) based on the orientation of their electric fields (E) relative to the aerial line connecting the Tx and Rx. We consider the electric field parallel to the aerial line as H polarization and the field perpendicular to the aerial line as the V polarization, although both polarizations lie in the horizontal plane. If the electrical field in the transmitter and receiver are perpendicular to each other, we refer to this as cross-polarization (HV or VH) otherwise it is co-polarization (HH or VV).

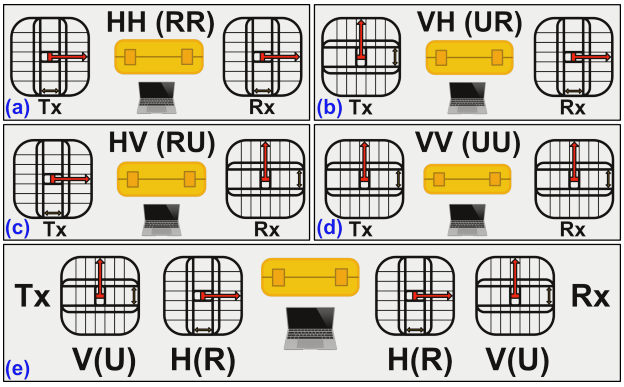

Fig. 2. Schematic bird's-eye view of pRES antenna configuration. H: Horizontal, V: Vertical, R: Right, U: Up are the direction fo the electric field in each antenna. (a-d) Step-by-step rotation for two antenna measurements. (e) MIMO mode configuration.

The full polarimetric response of the radar signal can be synthesized out of three (ideally four) measurements including the pairs HH, VV, and HV or VH as they are ideally the same [12]. In practice, these measurements can be collected in different ways depending on the polarity of the individual antennas. For the pRES antennas, the antenna polarity is uniquely determined by the directivity of the cable feeds (Fig. 2). We therefore suggest that the direction of the cables is recorded during data acquisition so that HH corresponds to right-right (RR) meaning that antenna cables are pointing rightwards relative to a pre-defined direction (e.g., the ice-flow direction or geographic North). All other measurements follow this terminology (i.e., HV corresponds to right-up and so on). This terminology removes ambiguities of the conventional H and V nomenclature and can also be applied in case only two antennas are available, so that the synthesis is achieved by counter-clockwise rotation of individual antennas (Fig. 2 a-e). We have found that a flipped antenna orientation (which corresponds to a 180-degree phase shift) may sometimes remain unnoticed in the post-processing and consequently lead to errors in determining both ice-fabric strength and the direction of the principal axis. In case the antennas require a different positioning, as was the case for this study due to cables length, then the phase needs to be corrected by 180 degrees (i.e. corresponding to a multiplication of the complex signal with -1) prior to further post-processing.

III. First Deployment Outcome

A. Study Area

This study showcases a proof-of-concept dataset derived from a 23 km long quad-polarimetric profile autonomously collected within the described setup. The dataset spans the grounding-zone of the Ekström Ice Shelf (Fig. 3), and was gathered with the logistical support of the Neumayer III station [34]. First deployment and initial testing was done next to the station. Subsequently, the rover was transported to the grounding line of the Ekström Ice Shelf, located approximately 120 km south of Neumayer III, initiating the data collection phase across the grounding zone (Fig. 3).

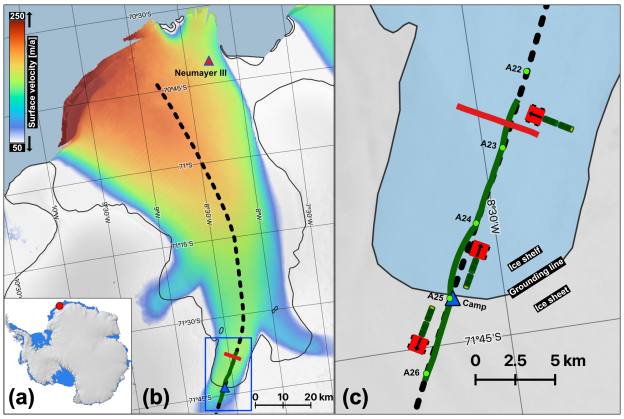

Fig. 3. (a) Location of Ekström ice shelf in Antarctica. (b) Surface flow velocity in Ekström ice shelf. Center flow line (dashed black line) The red triangle is the location of Neumayer station and the blue triangle is the location of the camp at the grounding line. (c) Location of the radar profiles at the grounding line. The blue area is the Ekström Ice Shelf, separated from the ice sheet (gray area) by the grounding line (solid black line). The green and red profiles are the SLEDGE collected data along and across the ice flow, respectively. The schematic of the rover shows in which direction the data were collected.

B. Data Acquisition

In January 2022, SLEDGE collected two profiles of quad-polarimetric pRES data ($\sim$ 450 points) over a total operational period of approximately 20 h (Table I). This includes mobility problems such as getting blocked by oversized sastrugi. Such problems happened approximately 10 times and were handled by the operator who was typically within 3 km range. This profile used the rubber wheel-setup (section III-D) with a pRES configured to collect all four polarizations with 10 stacks and 40 sub-bursts. The total measuring time at each location was approximately 1 minute. The rover was operated at a speed of 1 m/s which is approximately one third of the maximum speed.

TABLE I
SLEDGE OPERATIONAL TIME.

Date	Start	Finish	Duration [h]	Profile
03.01.2021	17:00	22:00	5	Along flow
04.01.2021	14:00	18:30	4:30	Along flow
05.01.2021	14:30	21:00	6:30	Along flow
06.01.2021	12:00	12:30	00:30	Along flow
06.01.2021	14:00	16:00	2	Across flow
06.01.2021	20:30	21:30	1	Along flow

The first profile is oriented along flow and extends over 18 km from A26 to ∼2 km before A22 (Fig. 3c – green line). The radar trace spacing between points A26 to A25 was 20 m, and 100 m elsewhere. The second profile extends in the across-flow direction (perpendicular to the A23-A22 profile) with 100 m trace spacing throughout (Fig. 3c – red line). We have also collected a 800 m profile at 1 m spacing (6 operational hours) with a lower-frequency version of the pRES (20-40 MHz) using the RTK positioning system. Results of this will be reported elsewhere.

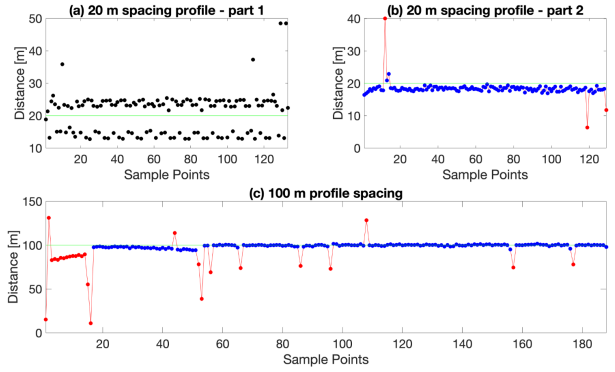

Fig. 4. The distance between two adjacent pRES measurement points. (a) First 1 km of the 20 m spacing target. (b) Rest of the 20 m spacing profile. (c) All the points with 100 m spacing target. The green lines are the target spacing. All the data in (a) and all the red points are the external problems and were neglected for the mean and standard deviation calculations. Note that (a) and (b) showing the data from A26 to A25 profile in Fig. 3 and (c) shows all the data collected along and across flow in 100 m spacing.

The first section (∼1 km) of the 20 m spacing profile (Fig. 3c, A25 to A26) suffers from oscillating positioning errors relative to the pre-defined locations with approximately ± 5 m (Fig. 4a). The source of this mismatch was linked to a wrongly initialized heading which was locally defined between the 20 m postings. Even a small angular uncertainty leads to an instable navigation due to the dependence of the system on using the GPS for determining its direction. This is improved when a single heading is defined using the far-end turning point of the profile. The spacing of individual radar measurements can then be defined using that heading and the along-track distance. The difference between both modes is evidenced in Fig. 4a where, by mistake, local headings were used for the first kilometer of the along flow profile. Changing the heading direction to the end of the profile reduced the positioning error with few exceptions (Fig. 4b) in strongly undulated terrain which we discuss further in section III-D. The same holds for the positioning at 100 m spacings both in along and across flow (Fig. 4c). An exception here occurs at waypoint A25 due to a wrong coordinate entry by the operator. For the bulk part of the profile, the deviation of observed positioning mismatch from the target is 1.2 ± 1.4 m (mean and standard deviation) which is within our expectations when operating the rover without the RTK. This will not impact the interpretation of the polarimetric radar data.

Due to limited cable lengths for the farther antennas, the need to avoid cable tension, and the potential for inconvenient cable positioning, the data were collected in a non-standard configuration. (Fig. 1) which requires the 180-phase correction on HH and HV (see sec. II-D). After that, each trace underwent polarimetric standard processing outlined by [12]. That means that for each location the standard ice-thickness (and in parts internal stratigraphy) product is supplemented with the full orientation dependence from which the ice-fabric types can be reconstructed. This is a significant step forward compared to a manual deployment of the antennas where typically only a few tens of measurements can be collected in about 20 h (compared to 450 using SLEDGE).

C. Showcasing the Collected Data

Here we show the quad-polarimetric dataset and highlight the potential for further scientific application. In all profiles, the ice-bedrock and ice-ocean interfaces can clearly be detected also including the transition of the grounding zone (Fig 5a). Internal reflection horizons are equally apparent, particularly in the 20 m spacings. In that sense SLEDGE provides similar results as pulsed ground-based radar systems in this area, albeit it requires a much longer acquisition time.

The added value of SLEDGE becomes apparent when evaluating the quad-polarimetric response which can be shown in different metrics such as backscattered power, power anomalies, coherence phase and its depth gradient. The backscattred power reveals the basal structures in all antenna combinations but with variable basal reflection amplitudes (Supplementary Information - Fig. SI-2, e.g, VH backscattered power shows a stronger contrast). The large-scale basal structures are the same for all polarization combinations, but at a trace-by-trace level differences occur that, at least in part, also image variable basal roughness due to the polarization dependent antenna footprint. Independent of backscattered power, we apply standard quad-polarimetric radar processing at each trace which is sensitive to the dielectric anisotropic and hence birefringent properties of ice. The coherence phase describes the correlation between the two co-polarized signals (HH and VV) and its depth gradient is indicative for the magnitude of ice fabric anisotropy [9], [10]. Power anomalies, which result from the constructive and destructive superposition of the ordinary and extra-ordinary waves, are used to infer the reflection ratio between layers (co-polarized power anomaly) and horizontal ice-fabric orientation (cross-polarized power anomaly). This enables the detection of depth-dependent ice-fabric types, both in terms of strength and orientation, in many flow regimes [12]. The full azimuthal illustration of the polarimetric response at each trace in both along-flow and across-flow profiles is shown in the Supplementary Information - Sec. 4 (Video in [35]).

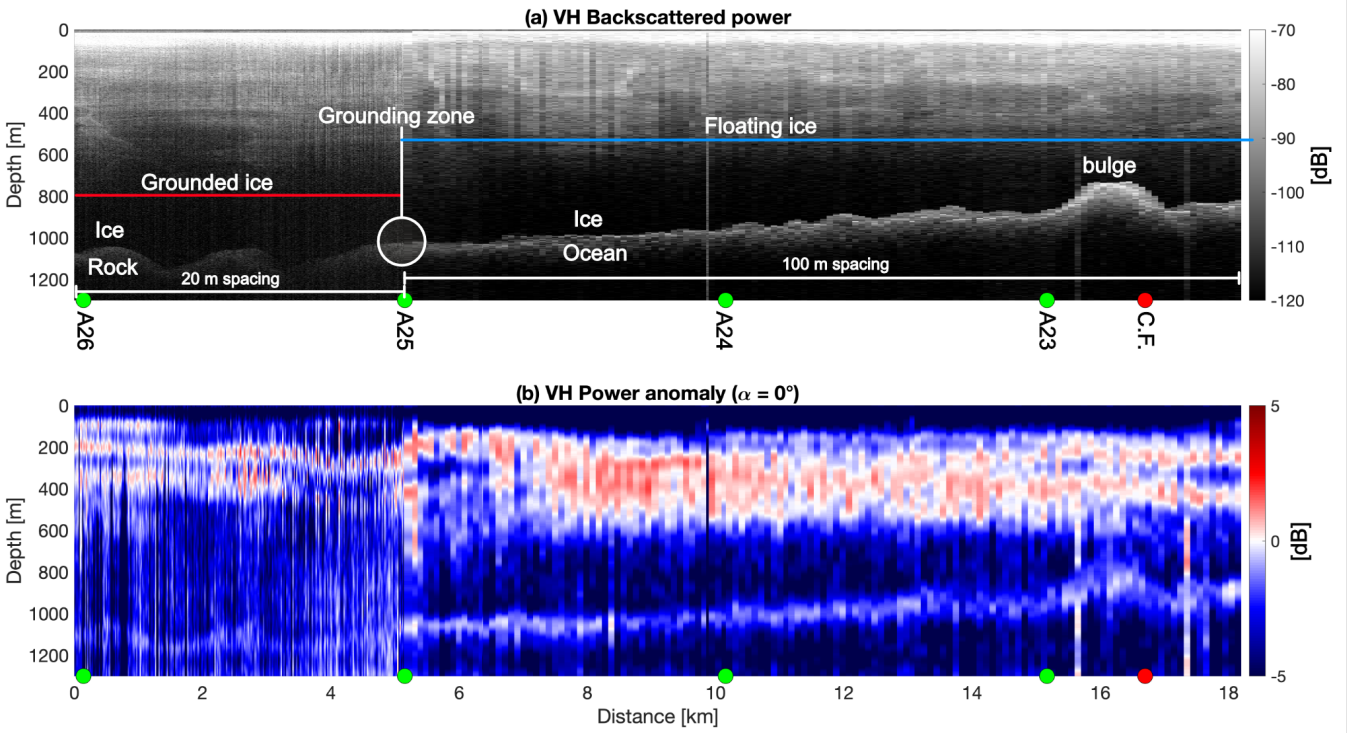

Fig. 5. Recorded data along the flow profile illustration the backscattered power and cross polarized power anomaly both for VH antenna combination. Note that the red circle marked as C.F. shows the location of the across flow profile.

The inference of ice-fabric patterns, including travel time analysis [20] and inversion [12] will be done in a different study. Here, we restrict ourselves to demonstrate the VH backscatter power (Fig. 5a) and the VH backscattered power anomaly extracted at an angle ($\alpha = 0$) parallel to the profile direction (Fig. 5b). Small values (i.e., the blue colors in Fig. 5b) indicate that one of the horizontal ice-fabric's principal axes is oriented along-flow. At shallower depths (i.e., the red colors) this is not the case, and we infer that the ice-fabric is rotated in this depth interval by approximately 45 degrees (Supporting Information Sec. 4 - video in [35]). This effect becomes progressively stronger just downstream of the landward limit from the grounding zone. The coherence phase shows a strongly depth-variable gradient with multiple nodes throughout the profile. This pattern is comparable to other locations with significant ice flow (e.g., the EDML ice core site [12]) and a stronger ice anisotropy as would be expected at, e.g., ice domes. Detecting such along-flow changes over many kilometers at 100 m spacings offers new possibilities for ground-based radar-polarimetric surveys which are of interest for ice-shelf [36] and ice-stream shear margins [11], [13].

D. Operational Challenges and Recommendations

The rover is equipped with two wheel sets. The first, metal grouser wheels, are tailored for snow surfaces, preventing submersion in soft snow (Fig. 6b) and enhancing traction on medium-sized sastrugi. However, in near-melting temperatures, snow accumulation inside and outside the wheels can lead to immobilization (Fig. 6a). In such conditions, the second set of rubber wheels performs better. Larger sastrugi (∼50 cm vertical) can also immobilize the rover due to sled weight (Fig. 6c). This was the biggest challenge preventing full autonomous operation.

The current transmission lacks sufficient torque to navigate sastrugi, especially when maneuvering the rover rapidly at sub-meter intervals and making frequent start-stop switches, crucial for scientific applications like SAR processing. To address this, a more robust transmission that delivers increased torque can effectively alleviate this issue. To ensure the rover maintains a straight trajectory toward its destination (Fig. 6d), revising the autonomous navigational algorithm along with adding a magnetometer sensor as a compass and direct feedback from rotary encoders on the wheels are recommended.

The pRES radar is not ruggedised for mobile use and the LAN connection between the rover and radar frequently disconnects, especially after traversing sastrugi. This can be improved by adding WIFI module to the pRES for wireless communication. Furthermore, the sleds used in deployments lacked brakes, resulting in occasional collisions with the rear of the rover. This can be prevented with including shock absorbers at the rover's rear. The sum of technical shortcomings and the difficult terrain with soft snow and frequent sastrugis prevented us to successfully deploy SLEDGE fully autonomous in overnight surveys. However, we believe that this will be possible in the future once the suggested improvements are implemented, and thus offer field teams another time efficient method of data collection.

IV. Conclusion

The integration of a phase-coherent, quad-polarimetric radar with an autonomous rover, demonstrated in a proof-of-concept

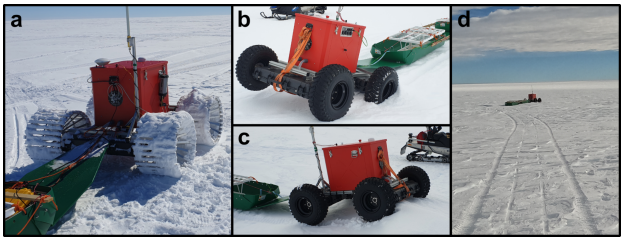

Fig. 6. (a) Substantial accumulation of snow on metal wheels. (b) The rover sinking into soft snow with rubber wheels. (c) The rover facing difficulties traversing sastrugi. (d) The rover starting to deviate from the straight line.

study in Antarctica, shows the system's capacity to collect quad-polarimetric data along extensive profiles, spanning up to 23 km in just 20 operational hours. This system now allows ground-based quad-polarimetric profiles to be collected at spacings previously unattainable. We've demonstrated this with transects in the grounding zone of the Ekström ice shelf. We suggest that the ice is more anisotropic compared to comparable measurements at the ice interior, and the ice-fabric direction rotates in some depth intervals across the grounding zone. These data are crucial for understanding the effects of the grounding line on ice fabric anisotropy, informing ice flow models, and unraveling the stress and strain history of the ice.

While presenting promising results, our first deployment observations highlight areas for improvement in future deployments. The most crucial ones, causing the most interruptions in data acquisition and requiring attention in the next deployment, are adjusting the transmission to provide more torque to navigate larger sastrugi, revising the autonomous navigational algorithm, and ensuring a reliable network connection between pRES and the rover.

Looking ahead, SLEDGE's versatility opens possibilities for attaching other radars or geophysical sensors, such as magnetic, gravimetry, and electric sensors, broadening its applicability beyond ice-fabric anisotropy studies.

Code and Data Availability

The rover (ROS2) and interface (MATLAB GIU) source code for SLEDGE. https://zenodo.org/records/10064669. pRES HTTP REST API. https://zenodo.org/records/10047461. pRES quad-polarimetric for field manual and code. https://zenodo.org/records/10064673. Data are available on PANGAEA database [37].

Author Contributions

MRE lead the code and hardware development of SLEDGE, data acquisition in the field and data processing. RD designed the study outline. OE supported the field test of SLEDGE. RD, JH, IK and OE supported the data acquisition in the field. JE and APL developed the original version of the rover (FROSTYBOY) and advised on hardware development for SLEDGE. All authors contributed to the writing and editing of the final paper.

Competing Interests

JE and APL are commercial robotic suppliers of the rover (FROSTYBOY) used in this study.

Acknowledgment

We would like to mention M. Reza Ershadi, Inka Koch, and Reinhard Drews were supported by Deutsche Forschungsgemeinschaft (DFG) Emmy Noether grant (grant no. DR 822/3-1) and Jonathan Hawkins' PhD was funded by Royal Society Enhancement Award number RGF\EA\180173. We would like to thank the GrouZe team and the logistic support from Neumayer III.

Financial Support

This research has been supported by Deutsche Forschungsgemeinschaft (DFG) Emmy Noether grant (grant no. DR 822/3-1).

References

[1] H. Seroussi, S. Nowicki, A. J. Payne, H. Goelzer, W. H. Lipscomb, A. Abe-Ouchi, C. Agosta, T. Albrecht, X. Asay-Davis, A. Barthel, R. Calov, R. Cullather, C. Dumas, B. K. Galton-Fenzi, R. Gladstone, N. R. Golledge, J. M. Gregory, R. Greve, T. Hattermann, M. J. Hoffman, A. Humbert, P. Huybrechts, N. C. Jourdain, T. Kleiner, E. Larour, G. R. Leguy, D. P. Lowry, C. M. Little, M. Morlighem, F. Pattyn, T. Pelle, S. F. Price, A. Quiquet, R. Reese, N.-J. Schlegel, A. Shepherd, E. Simon, R. S. Smith, F. Straneo, S. Sun, L. D. Trusel, J. Van Breedam, R. S. W. van de Wal, R. Winkelmann, C. Zhao, T. Zhang, and T. Zwinger, "ISMIP6 Antarctica: a multi-model ensemble of the Antarctic ice sheet evolution over the 21st century," *The Cryosphere*, vol. 14, no. 9, pp. 3033–3070, Sep. 2020, publisher: Copernicus GmbH. [Online]. Available: https://tc.copernicus.org/articles/14/3033/2020/

[2] S. H. Faria, I. Weikusat, and N. Azuma, "The microstructure of polar ice. Part II: State of the art," *Journal of Structural Geology*, vol. 61, pp. 21–49, Apr. 2014. [Online]. Available: https://linkinghub.elsevier.com/retrieve/pii/S0191814113002009

[3] I. Weikusat, D. Jansen, T. Binder, J. Eichler, S. H. Faria, F. Wilhelms, S. Kipfstuhl, S. Sheldon, H. Miller, D. Dahl-Jensen, and T. Kleiner, "Physical analysis of an Antarctic ice core—towards an integration of micro- and macrodynamics of polar ice," *Philosophical Transactions of the Royal Society A: Mathematical, Physical and Engineering Sciences*, vol. 375, no. 2086, p. 20150347, Feb. 2017. [Online]. Available: https://royalsocietypublishing.org/doi/10.1098/rsta.2015.0347

[4] N. D. Hargreaves, "The polarization of radio signals in the radio echo sounding of ice sheets," *Journal of Physics D: Applied Physics*, vol. 10, no. 9, pp. 1285–1304, Jun. 1977. [Online]. Available: https://iopscience.iop.org/article/10.1088/0022-3727/10/9/012

[5] ——, "The radio-frequency birefringence of polar ice," *Journal of Glaciology*, vol. 21, no. 85, pp. 301–313, 1978, publisher: Cambridge University Press. [Online]. Available: https://www.cambridge.org/core/journals/journal-of-glaciology/article/radiofrequency-birefringence-of-polar-ice/5BCE70F0B63DEFDC609FE973F377394F

[6] S. Fujita, H. Maeno, S. Uratsuka, T. Furukawa, S. Mae, Y. Fujii, and O. Watanabe, "Nature of radio echo layering in the Antarctic Ice Sheet detected by a two-frequency experiment," *Journal of Geophysical Research: Solid Earth*, vol. 104, no. B6, pp. 13 013–13 024, Jun. 1999. [Online]. Available: http://doi.wiley.com/10.1029/1999JB900034

[7] S. Fujita, H. Maeno, and K. Matsuoka, "Radio-wave depolarization and scattering within ice sheets: a matrix-based model to link radar and ice-core measurements and its application," *Journal of Glaciology*, vol. 52, no. 178, pp. 407–424, 2006. [Online]. Available: https://www.cambridge.org/core/product/identifier/S0022143000211702/type/journal_article

[8] O. Eisen, I. Hamann, S. Kipfstuhl, D. Steinhage, and F. Wilhelms, "Direct evidence for continuous radar reflector originating from changes in crystal-orientation fabric," *The Cryosphere*, vol. 1, no. 1, pp. 1–10, Oct. 2007. [Online]. Available: https://tc.copernicus.org/articles/1/1/2007/

[9] T. M. Jordan, D. M. Schroeder, D. Castelletti, J. Li, and J. Dall, "A Polarimetric Coherence Method to Determine Ice Crystal Orientation Fabric From Radar Sounding: Application to the NEEM Ice Core Region," *IEEE Transactions on Geoscience and Remote Sensing*, vol. 57, no. 11, pp. 8641–8657, Nov. 2019. [Online]. Available: https://ieeexplore.ieee.org/document/8755860/

[10] T. M. Jordan, D. M. Schroeder, C. W. Elsworth, and M. R. Siegfried, "Estimation of ice fabric within Whillans Ice Stream using polarimetric phase-sensitive radar sounding," *Annals of Glaciology*, vol. 61, no. 81, pp. 74–83, Apr. 2020. [Online]. Available: https://www.cambridge.org/core/product/identifier/S0260305520000063/type/journal_article

[11] T. J. Young, C. Martín, P. Christoffersen, D. M. Schroeder, S. M. Tulaczyk, and E. J. Dawson, "Rapid and accurate polarimetric radar measurements of ice crystal fabric orientation at the western antarctic ice sheet (wais) divide ice core site," *The Cryosphere*, vol. 15, no. 8, pp. 4117–4133, 2021. [Online]. Available: https://tc.copernicus.org/articles/15/4117/2021/

[12] M. R. Ershadi, R. Drews, C. Martín, O. Eisen, C. Ritz, H. Corr, J. Christmann, O. Zeising, A. Humbert, and R. Mulvaney, "Polarimetric radar reveals the spatial distribution of ice fabric at domes and divides in East Antarctica," *The Cryosphere*, vol. 16, no. 5, pp. 1719–1739, May 2022, publisher: Copernicus GmbH. [Online]. Available: https://tc.copernicus.org/articles/16/1719/2022/

[13] T. A. Gerber, D. A. Lilien, N. M. Rathmann, S. Franke, T. J. Young, F. Valero-Delgado, M. R. Ershadi, R. Drews, O. Zeising, A. Humbert, N. Stoll, I. Weikusat, A. Grinsted, C. S. Hvidberg, D. Jansen, H. Miller, V. Helm, D. Steinhage, C. O'Neill, J. Paden, S. P. Gogineni, D. Dahl-Jensen, and O. Eisen, "Crystal orientation fabric anisotropy causes directional hardening of the Northeast Greenland Ice Stream," *Nature Communications*, vol. 14, no. 1, p. 2653, May 2023, number: 1 Publisher: Nature Publishing Group. [Online]. Available: https://www.nature.com/articles/s41467-023-38139-8

[14] P. V. Brennan, L. B. Lok, K. Nicholls, and H. Corr, "Phase-sensitive FMCW radar system for high-precision Antarctic ice shelf profile monitoring," *IET Radar, Sonar & Navigation*, vol. 8, no. 7, pp. 776–786, Aug. 2014. [Online]. Available: https://onlinelibrary.wiley.com/doi/10.1049/iet-rsn.2013.0053

[15] K. W. Nicholls, H. F. Corr, C. L. Stewart, L. B. Lok, P. V. Brennan, and D. G. Vaughan, "A ground-based radar for measuring vertical strain rates and time-varying basal melt rates in ice sheets and shelves," *Journal of Glaciology*, vol. 61, no. 230, pp. 1079–1087, 2015. [Online]. Available: https://www.cambridge.org/core/product/identifier/S0022143000200269/type/journal_article

[16] O. Zeising, D. Steinhage, K. W. Nicholls, H. F. J. Corr, C. L. Stewart, and A. Humbert, "Basal melt of the southern Filchner Ice Shelf, Antarctica," *The Cryosphere*, vol. 16, no. 4, pp. 1469–1482, Apr. 2022, publisher: Copernicus GmbH. [Online]. Available: https://tc.copernicus.org/articles/16/1469/2022/

[17] E. Case and J. Kingslake, "Phase-sensitive radar as a tool for measuring firn compaction," *Journal of Glaciology*, pp. 1–14, Aug. 2021, publisher: Cambridge University Press. [Online]. Available: https://www.cambridge.org/core/journals/journal-of-glaciology/article/phasesensitive-radar-as-a-tool-for-measuring-firn-compaction/6400A1F1341117C72042EFC96DCE7234

[18] J. Kingslake, R. C. A. Hindmarsh, G. Aðalgeirsdóttir, H. Conway, H. F. J. Corr, F. Gillet-Chaulet, C. Martín, E. C. King, R. Mulvaney, and H. D. Pritchard, "Full-depth englacial vertical ice sheet velocities measured using phase-sensitive radar," *Journal of Geophysical Research: Earth Surface*, vol. 119, no. 12, pp. 2604–2618, 2014.

[19] F. Gillet-Chaulet, R. C. A. Hindmarsh, H. F. J. Corr, E. C. King, and A. Jenkins, "In-situ quantification of ice rheology and direct measurement of the Raymond Effect at Summit, Greenland using a phase-sensitive radar: *IN-SITU* QUANTIFICATION OF ICE RHEOLOGY," *Geophysical Research Letters*, vol. 38, no. 24, pp. n/a–n/a, Dec. 2011. [Online]. Available: http://doi.wiley.com/10.1029/2011GL049843

[20] O. Zeising, T. A. Gerber, O. Eisen, M. R. Ershadi, N. Stoll, I. Weikusat, and A. Humbert, "Improved estimation of the bulk ice crystal fabric asymmetry from polarimetric phase co-registration," *The Cryosphere*, vol. 17, no. 3, pp. 1097–1105, Mar. 2023, publisher: Copernicus GmbH. [Online]. Available: https://tc.copernicus.org/articles/17/1097/2023/

[21] E. Trautmann, L. Ray, and J. Lever, "Development of an autonomous robot for ground penetrating radar surveys of polar ice," in *2009 IEEE/RSJ International Conference on Intelligent Robots and Systems*, Oct. 2009, pp. 1685–1690, iSSN: 2153-0866. [Online]. Available: https://ieeexplore.ieee.org/document/5354290

[22] A. O. Hoffman, H. C. Steen-Larsen, K. Christianson, and C. Hvidberg, "A low-cost autonomous rover for polar science," *Geoscientific Instrumentation, Methods and Data Systems*, vol. 8, no. 1, pp. 149–159, Jun. 2019, publisher: Copernicus GmbH. [Online]. Available: https://gi.copernicus.org/articles/8/149/2019/

[23] K. D. Mankoff, D. v. As, A. Lines, T. Bording, J. Elliott, R. Kraghede, H. Cantalloube, H. Oriot, P. Dubois-Fernandez, O. R. d. Plessis, A. V. Christiansen, E. Auken, K. Hansen, W. Colgan, and N. B. Karlsson, "Search and recovery of aircraft parts in ice-sheet crevasse fields using airborne and in situ geophysical sensors," *Journal of Glaciology*, vol. 66, no. 257, pp. 496–508, Jun. 2020, publisher: Cambridge University Press.

[24] S. A. Arcone, J. H. Lever, L. E. Ray, B. S. Walker, G. Hamilton, and L. Kaluzienski, "Ground-penetrating radar profiles of the McMurdo Shear Zone, Antarctica, acquired with an unmanned rover: Interpretation of crevasses, fractures, and folds within firn and marine ice," *Geophysics*, Sep. 2015, publisher: Society of Exploration Geophysicists. [Online]. Available: https://library.seg.org/doi/10.1190/geo2015-0132.1

[25] L. Ray, A. Adolph, A. Morlock, B. Walker, M. Albert, J. H. Lever, and J. Dibb, "Autonomous rover for polar science support and remote sensing," in *2014 IEEE Geoscience and Remote Sensing Symposium*, Jul. 2014, pp. 4101–4104, iSSN: 2153-7003. [Online]. Available: https://ieeexplore.ieee.org/document/6947388

[26] S.-E. Hamran, D. A. Paige, H. E. F. Amundsen, T. Berger, S. Brovoll, L. Carter, L. Damsgård, H. Dypvik, J. Eide, S. Eide, R. Ghent, Ø. Helleren, J. Kohler, M. Mellon, D. C. Nunes, D. Plettemeier, K. Rowe, P. Russell, and M. J. Øyan, "Radar Imager for Mars' Subsurface Experiment—RIMFAX," *Space Science Reviews*, vol. 216, no. 8, p. 128, Nov. 2020. [Online]. Available: https://doi.org/10.1007/s11214-020-00740-4

[27] I. Koch, R. Drews, S. Franke, D. Jansen, F. M. Oraschewski, L. S. Muhle, V. Višnjević, K. Matsuoka, F. Pattyn, and O. Eisen, "Radar internal reflection horizons from multisystem data reflect ice dynamic and surface accumulation history along the princess ragnhild coast, dronning maud land, east antarctica," *Journal of Glaciology*, p. 1–19, 2023.

[28] P. Dutrieux, C. Stewart, A. Jenkins, K. W. Nicholls, H. F. J. Corr, E. Rignot, and K. Steffen, "Basal terraces on melting ice shelves," *Geophysical Research Letters*, vol. 41, no. 15, pp. 5506–5513, 2014, _eprint: https://onlinelibrary.wiley.com/doi/pdf/10.1002/2014GL060618. [Online]. Available: https://onlinelibrary.wiley.com/doi/abs/10.1002/2014GL060618

[29] R. Drews, F. Pattyn, I. J. Hewitt, F. S. L. Ng, S. Berger, K. Matsuoka, V. Helm, N. Bergeot, L. Favier, and N. Neckel, "Actively evolving subglacial conduits and eskers initiate ice shelf channels at an Antarctic grounding line," *Nature Communications*, vol. 8, no. 1, p. 15228, May 2017, number: 1 Publisher: Nature Publishing Group. [Online]. Available: https://www.nature.com/articles/ncomms15228

[30] G. Church, M. Grab, C. Schmelzbach, A. Bauder, and H. Maurer, "Monitoring the seasonal changes of an englacial conduit network using repeated ground-penetrating radar measurements," *The Cryosphere*, vol. 14, no. 10, pp. 3269–3286, Oct. 2020, publisher: Copernicus GmbH. [Online]. Available: https://tc.copernicus.org/articles/14/3269/2020/

[31] A. P. Lines, J. J. Elliott, and L. E. Ray, "Incipient Immobilization Detection for Lightweight Rovers Operating in Deformable Terrain," *Journal of Autonomous Vehicles and Systems*, vol. 2, no. 3, p. 031001, 01 2023. [Online]. Available: https://doi.org/10.1115/1.4056408

[32] S. Macenski, T. Foote, B. Gerkey, C. Lalancette, and W. Woodall, "Robot Operating System 2: Design, architecture, and uses in the wild," *Science Robotics*, vol. 7, no. 66, p. eabm6074, May 2022, publisher: American Association for the Advancement of Science. [Online]. Available: https://www.science.org/doi/10.1126/scirobotics.abm6074

[33] J. Dall, "Ice sheet anisotropy measured with polarimetric ice sounding radar," in *2010 IEEE International Geoscience and Remote Sensing Symposium*. Honolulu, HI, USA: IEEE, Jul. 2010, pp. 2507–2510. [Online]. Available: http://ieeexplore.ieee.org/document/5653528/

[34] C. Wesche, R. Weller, G. König-Langlo, T. Fromm, A. Eckstaller, U. Nixdorf, and E. Kohlberg, "Neumayer III and Kohnen Station in Antarctica operated by the Alfred Wegener Institute," *Journal of large-scale research facilities JLSRF*, vol. 2, pp. A85–A85, Aug. 2016. [Online]. Available: https://jlsrf.org/index.php/lsf/article/view/152

[35] M. R. Ershadi, R. Drews, J. Hawkins, J. Elliott, A. P. Lines, I. Koch, and O. Eisen, "Dataset - autonomous rover enables radar profiling of ice-fabric properties in antarctica," 2024. [Online]. Available: https://dx.doi.org/10.21227/9twx-eb68

[36] D. A. Lilien, N. M. Rathmann, C. S. Hvidberg, A. Grinsted, M. R. Ershadi, R. Drews, and D. Dahl-Jensen, "Simulating higher-order fabric structure in a coupled, anisotropic ice-flow model: application to dome c," *Journal of Glaciology*, p. 1–20, 2023.

[37] M. R. Ershadi, R. Drews, J. Hawkins, J. Elliott, A. P. Lines, I. Koch, and O. Eisen, "Quad-polarimetric pRES Data Collected at the Ekström Ice Shelf Grounding Zone, East Antarctica," 2024. [Online]. Available: https://doi.org/10.1594/PANGAEA.965555